Design and application of ion-implanted polySi passivating contacts for interdigitated back contact c-Si solar cells

Yang, Guangtao; Ingenito, Andrea; van Hameren, Nienke; Isabella, Olindo; Zeman, Miro

DOI
10.1063/1.4940364

Publication date
2016

Document Version
Final published version

Published in
Applied Physics Letters

Design and application of ion-implanted polySi passivating contacts for interdigitated back contact c-Si solar cells

Guangtao Yang, Andrea Ingenito, Nienke van Hameren, Olindo Isabella, and Miro Zeman

Citation: Appl. Phys. Lett. **108**, 033903 (2016); doi: 10.1063/1.4940364
View online: http://dx.doi.org/10.1063/1.4940364
View Table of Contents: http://aip.scitation.org/toc/apl/108/3
Published by the American Institute of Physics

Design and application of ion-implanted polySi passivating contacts for interdigitated back contact c-Si solar cells

Guangtao Yang, Andrea Ingenito, Nienke van Hameren, Olindo Isabella, and Miro Zeman
PVMD, Delft University of Technology, P.O. Box 5031, 2600 GA Delft, The Netherlands

(Received 3 November 2015; accepted 6 January 2016; published online 20 January 2016)

Ion-implanted passivating contacts based on poly-crystalline silicon (polySi) are enabled by tunneling oxide, optimized, and used to fabricate interdigitated back contact (IBC) solar cells. Both n-type (phosphorous doped) and p-type (boron doped) passivating contacts are fabricated by ion-implantation of intrinsic polySi layers deposited via low-pressure chemical vapor deposition and subsequently annealed. The impact of doping profile on the passivation quality of the polySi doped contacts is studied for both polarities. It was found that an excellent surface passivation could be obtained by confining as much as possible the implanted-and-activated dopants within the polySi layers. The doping profile in the polySi was controlled by modifying the polySi thickness, the energy and dose of ion-implantation, and the temperature and time of annealing. An implied open-circuit voltage of 721 mV for n-type and 692 mV for p-type passivating contacts was achieved. Besides the high passivating quality, the developed passivating contacts exhibit reasonable high conductivity ($R_{sh\,n\text{-}type} = 95\ \Omega/\square$ and $R_{sh\,p\text{-}type} = 120\,\Omega/\square$). An efficiency of 19.2% ($V_{oc} = 673$ mV, $J_{sc} = 38.0$ mA/cm^2, $FF = 75.2\%$, and *pseudo-FF* $= 83.2\%$) was achieved on a front-textured IBC solar cell with polySi passivating contacts as both back surface field and emitter. By improving the front-side passivation, a V_{OC} of 696 mV was also measured. © *2016 AIP Publishing LLC*.
[http://dx.doi.org/10.1063/1.4940364]

Crystalline silicon (c-Si) solar cells technology has been continuously improved in both material quality and surface passivation. This has resulted in an ample reduction of recombination losses at both bulk and surface level. Therefore, contact recombination is currently the limiting factor for achieving high efficiency. Carrier selective contacts have been proposed as valid candidates to suppress minority carrier recombination at contact, while still enabling majority carrier transport.[1] A carrier-selective contact is constituted by a material, which (i) exhibits excellent interface passivation, (ii) shows high carrier selectivity, (iii) creates a sufficient band bending, which separates the quasi Fermi-levels, to enable high built-in voltage, and (iv) enables majority-carriers transport. An example of such an approach is the heterojunction solar cells technology based on thin hydrogenated amorphous silicon (a-Si:H) layer.[2] With this solar cell architecture, high open circuit voltage (V_{oc}) up to 750 mV has been demonstrated, due to the excellent passivation by a-Si:H of the c-Si surface and the optimized interfaces of doped a-Si:H to the transparent conductive oxide (TCO) layer. However, a TCO layer is needed for properly contacting the a-Si:H layers. Moreover, the temperature tolerance of the a-Si:H passivation layer (<250 °C) limits the back-end process of the solar cells, which would need higher temperature, e.g., more transparent TCO layers, metallization step, and/or post-annealing step. Another example of carrier-selective contact is semi-insulating poly-crystalline silicon (SIPOS), which is a mixture of microcrystalline silicon and silicon oxide (SiO_x). By using such a technique excellent passivation of c-Si surface and a V_{oc} as high as 720 mV was obtained for the wafer-based c-Si solar cell structure n^+-SIPOS/thin SiO_2/p-type c-Si/thin SiO_2/n^+-SIPOS.[3] The tunneling oxide passivating contact (TOPCon) as carrier-selective contact has lately gained great interest in passivated emitter rear cell (PERC) c-Si solar cell architecture due to its excellent passivation and junction properties. The main features of the TOPCon approach are (i) a tunneling oxide layer and (ii) a doped poly-crystalline silicon (polySi).[4,5] A solar cell structure with full area n-type TOPCon on the back side and diffused boron emitter on the front enabling high open circuit voltage ($V_{oc} = 718$ mV) and high fill factor (fill factor $FF = 83.2\%$)[5] has been demonstrated at Fraunhofer ISE. The same group has also reported the application of such a concept in interdigitated back contact (IBC) solar cell with TOPCon on the back side as both emitter and back surface field (BSF). However, for such a solar cell, only the *Voc* (*Voc* = 682 mV) and *pseudo-FF* (*pFF* = 82.2%) measured using Suns-V_{oc}[6] were reported. The usage of ion-implanted polySi as potential passivating contacts for c-Si solar cells has been also recently reported.[7,8] In such contributions, the authors have calculated the iV_{OC} and the *pFF* based on dark-saturation current measured with Quasi-Steady State Photoconductance (QSSPC)[7,8] or have reported the potential V_{OC} and *FF* of an IBC solar-cell device with polySi passivating contacts based on the measured V_{OC} and *FF* of the front back contacted solar cell structures.[9]

In this letter, we show the development of ion-implanted polySi n-type and p-type passivating contacts and their implementation at the back side of IBC solar cells. In such architecture, both TOPCon-based BSF and emitter are located on the back side of the cell, which minimizes the parasitic optical absorption of these heavily doped polySi layers. A schematic illustration of the solar cell structure is shown in Fig. 1(a). For all experiments performed in this work, we used high quality n-type Float-Zone (FZ) c-Si wafer (thickness: 280 ± 20 μm thick, orientation: ⟨100⟩, and resistivity:

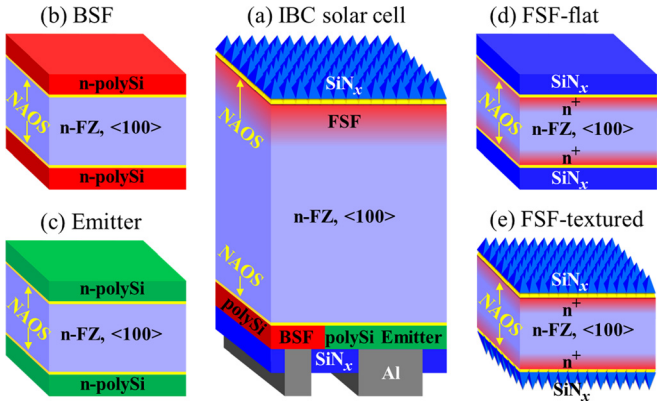

FIG. 1. (a) Schematic illustration of the front-textured interdigitated back contact (IBC) silicon solar cell with ion-implanted LP-CVD polycrystalline silicon (polySi) based tunnel oxide passivating contacts (TOPCon) as both emitter and back surface field (BSF). At the front side of the cell is the ion-implanted crystalline silicon (c-Si) as the front surface field (FSF), which is passivated by nitric acid oxidation of silicon (NAOS) and SiN_x. Symmetrical test structures are also sketched for (b) polySi BSF, (c) polySi emitter, and homojunction P-implanted (d) flat FSF and (f) textured FSF, which are passivated by nitric acid oxidation of silicon (NAOS)/SiN_x.

1–5 Ω cm). Focusing on solar cells fabrication, the c-Si wafer is cleaned in HNO_3 (99%), to remove eventual organic contaminations, and then in HNO_3 (68%, at 110 °C) to remove inorganic contaminations. During these cleaning steps, an ultra-thin SiO_2 layer is formed on each side of the c-Si wafer, which is also referred to as nitric acid oxidation of silicon (NAOS). The polySi layers used at the back side of the cell are deposited at 580 °C by low pressure chemical vapor deposition (LP-CVD) with a thickness of 250 nm. Boron (B) and phosphorous (P) dopants are locally ion-implanted into the polySi for emitter and BSF, respectively, for cell's fabrication. A P-implanted c-Si front surface field (FSF) is deployed at the front side of the cell. A subsequent high temperature annealing, at 950 °C for 5 min, is used to activate and drive-in both types of dopants at both front and back side in one step. On the front side, a NAOS layer and a SiN_x layer with thickness of 80-nm are deposited by plasma enhanced chemical vapor deposition (PE-CVD) with a double role of passivation layers for the FSF and antireflection coating. On the rear side, 80-nm thick PE-CVD SiN_x is deposited in order to enhance the internal rear reflectance. Finally, a lithographic step is used to define the contacts followed by Al evaporation (2 μm) and lift-off in acetone. The development of this process flow is based on the so-called self-aligned process for homo-junction IBC solar cells developed at TUDelft.[10]

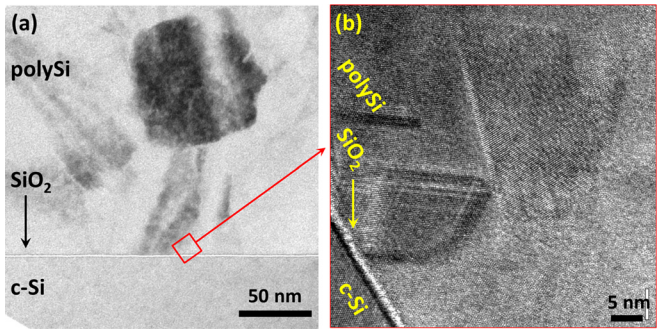

FIG. 2. (a) Transmission electron microscopy (TEM) image of a B-doped polySi passivating contact; (b) zoom-in at the polySi/NAOS/c-Si interfaces.

Alongside the realized solar cells, also symmetrical samples were fabricated in order to evaluate the passivation quality of the TOPCon layers. The structure of the symmetrical sample is doped-polySi/NAOS/c-Si/NAOS/doped-polySi and is schematically shown in Figs. 1(b) and 1(c) for P and B doping, respectively. After the NAOS and the dual-sided a-Si layer deposition, ion-implantation is performed on both sides of the wafer. Detailed information on the ion-implantation process (i.e., energy and dose) for a few selected samples is given in Table I. After implantation, a high temperature annealing step (5 min at 950 °C) is used to crystallize the a-Si layers into polySi and to activate/drive-in the dopants. Transmission electron microscopy (TEM) was used to visually evaluate the structure of the a-Si after the annealing. As shown in Fig. 2, after annealing, the a-Si is crystallized in polySi layer, exhibiting a wide grain size distribution ranging between 10 nm and >100 nm. To quantify the crystallinity fraction of the polySi, measurements based on Raman spectroscopy were performed, showing a crystallinity fraction of more than 90%. The thickness of the thin SiO_2 layer is ~1.5 nm, which can be recognized in Fig. 2(b). Passivation properties, such as effective minority-carrier lifetime (τ_{eff}), dark saturation current-density (J_0), and iV_{oc}, are reported in Table I. These were evaluated by using QSSPC method with a Sinton WCT120 lifetime tester.[11] Four probe measurements and transmission line method (TLM) were used to obtain the sheet resistance (R_{sh}) of the passivating contacts and the contact resistance (R_c) between such passivating contacts and the

TABLE I. Minority-carriers effective lifetime (τ_{eff}), dark saturation current-density (J_0), sheet resistance (R_{sh}), and implied V_{oc} (iV_{oc}) of the ion-implanted polySi passivating contacts and of the FSF used in our IBC cell.

Sample type	Sample number	Implantation energy (keV)	Implantation dose (cm^{-2})	τ_{eff} (ms)	J_0 (fA/cm^2)	R_{sh}[a] (Ω/□)	iV_{oc} (mV)
polySi-BSF	BSF-1	20	1×10^{16}	0.32	228	55	667
	BSF-2	20	5×10^{15}	9.44	8	95	721
	BSF-3	20	2×10^{15}	1.13	24	800	679
polySi-emitter	Emitter-1	20	5×10^{15}	2.23	31	120	692
	Emitter-2	20	1×10^{16}	1.12	65	120	677
FSF-flat[b]	FSF-1	20	5×10^{14}	0.33	138	245	654
FSF-textured[b]	FSF-2	20	5×10^{14}	0.27	192	356	638

[a]R_{sh} values are obtained by means of 4-point probe measurements from samples whose c-Si bulk has the opposite doping than the passivating contact under test.
[b]FSF is passivated by NAOS/SiN_x; R_{sh} values are obtained by means of 4-point probe measurements of FSF on a p-type c-Si wafer.

evaporated Al, respectively. In order to ensure an accurate measurement, the c-Si bulk used for the R_{sh} and R_c measurements exhibited opposite doping type than the one of the passivating contacts under test.

In this work, we optimized the electrical properties of the passivating contacts by varying the thickness of as-deposited a-Si layers, the energy and dose of the ion-implantation, and the temperature and time of the annealing. We find that these parameters are correlated to each other, when pursuing the right balance between passivation and conductivity eventually exhibited by optimized polySi passivating contacts. For example, the doping profile of the polySi passivating contacts can be controlled by tuning the implantation energy and dose. However, also the temperature and time of annealing play a role in the resulting doping profile. It is observed that, when confining most of the ion-implanted dopants within the polySi layer, a high τ_{eff} can be obtained. Realizing a P-doping profile mostly constant in the polySi material with a rapid drop within the c-Si bulk, as in case of BSF-2 (see Fig. 3), enables $\tau_{eff} = 9.4$ ms and $J_0 = 8$ fA/cm^2 (other parameters are listed in Table I). However, when P diffuses too deep into the c-Si bulk, e.g., BSF-1 in Fig. 3, there is a rapid drop in the passivation effect (see BSF-1 values in Table I). The physics behind this effect is not yet well understood, we suggest the following explanations: (1) The c-Si at the interface between c-Si bulk and the NAOS/polySi becomes a heavily doped n^{++} region due to the P in-diffusion inducing a strong increase of the Auger recombination rate; (2) this heavily doped region also dis-functions the carrier selectivity of the passivating contacts due to insufficient quasi Fermi level separation at bulk/polySi interface; and (3) the pin-holes in the tunneling oxide layer due to the high temperature process may also increase the oxide layer interface trap density, therefore, increase the SiO_2/c-Si interface recombination, which is considered as the dominating recombination mechanism.[7,12] All in all, the concurrent combination of these effects may enhance carrier recombination. To clarify the mechanism, further studies are required. Finally, when the P doping profile is too shallow within the polySi layer, e.g., BSF-3 shown in Fig. 3, the passivating effect is also poorer than in case of BSF-2 (see also Table I). This is because of the fact that when there is insufficient doping concentration at the polySi/Si interface there will not be enough band-bending to create a high built-in voltage. At the same time, because of this insufficient doping in the polySi layer, a high R_{sh} value, 800 Ω/□, is obtained. Although a similar behavior can be recognized in the realized p-type polySi passivating contacts (see both Fig. 4 and Table I), more investigation is required to understand the mechanism involved.

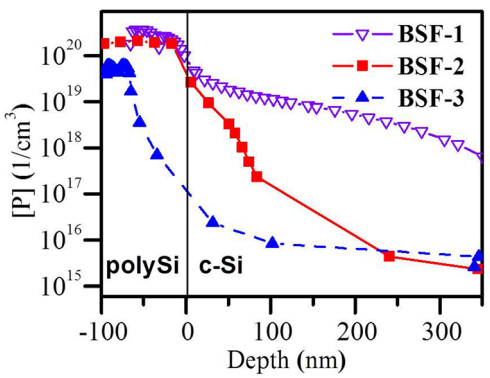

FIG. 3. P-doping profile measured by electrochemical capacitance-voltage (ECV) of three P-implanted polySi passivating contacts (BSF candidates in our IBC solar cell).

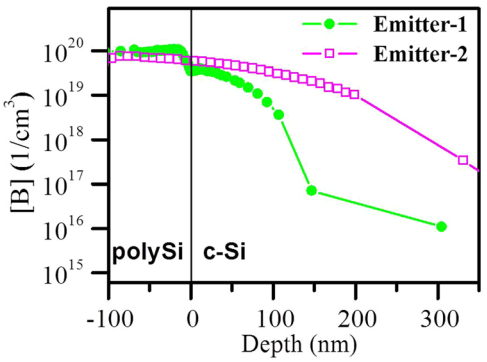

FIG. 4. B-doping profile measured by ECV for two B-implanted polySi passivating contacts (emitter candidates in our IBC solar cell).

The optimized polySi passivating contacts were used to demonstrate an IBC solar cells architecture with passivating carrier-selective contacts (see Fig. 1(a)). In particular, BSF-2 and emitter-1 were chosen as rear passivating contacts due to their high passivation quality and conductivity. The front side of the IBC c-Si solar cell was passivated by using the implanted FSF-1 (for flat cell) and FSF-2 (for front-textured cell) coated with NAOS/SiN_x stack (see Figs. 1(d) and 1(e), respectively, and Table I).

The IBC solar cells with polySi passivating contacts achieved a conversion efficiency of 18.2% in the case of flat front side and 19.2% in the case of textured front side. The external parameters of these 3×3-cm^2 wide cells were measured by using a class AAA Wacom WXS-156S solar simulator and are summarized in Table II. The calibration cells for both *J-V* and external quantum efficiency (*EQE*) measurements were calibrated at Fraunhofer Institute for Solar Energy Systems. As reported in Table II, a V_{oc} of 680 mV for the flat FSF-cell and 673 mV for the textured FSF-cell both passivated with NAOS/SiN_x were measured. The high *pFF* values (>83%) recorded at device level demonstrate that the fabrication method for patterning the BSF and emitter on the rear side does not lead to leakage currents or shunting paths. The relatively low *FF* (75.2%, for the best cell) is, therefore, mainly attributed to the high R_{sh} and low carrier mobility in the polySi layers rather than their contact resistance values, especially for the emitter. In fact, the measured contact resistance via TLM for the BSF and emitter were $R_{c\text{-BSF}} = 2.5\,\text{m}\Omega\,\text{cm}^2$ and $R_{c\text{-emitter}} = 1.4\,\text{m}\Omega\,\text{cm}^2$,

TABLE II. The illuminated *J-V* measurement of 9-cm^2 wide flat IBC solar cells with polySi emitter and BSF and NAOS/SiN_x passivated P-implanted FSF. The short-circuit current density (J_{sc}) values are obtained from the EQE measurement, while *pFF* are from Suns-V_{oc}-I50, illumination-Voltage tester, Sinton.

Cell	Front-side/passivation	V_{oc} (mV)	J_{sc} (mA/cm^2)	*FF* (%)	*pFF* (%)	η (%)
Flat	FSF/NAOS/SiN_x	680	35.9	74.5	83.7	18.2
Textured	FSF/NAOS/SiN_x	673	38.0	75.2	83.2	19.2

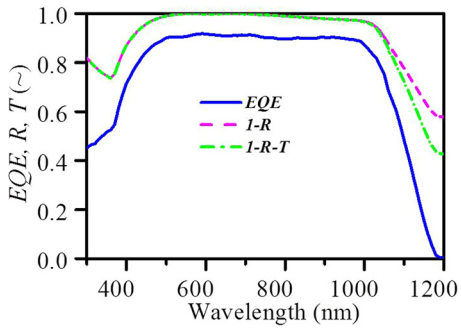

FIG. 5. The external and internal quantum efficiency (EQE, IQE) of the best IBC solar cell. Reflectance (R) and transmittance (T) are plotted as 1-R and 1-R-T, respectively.

respectively. An additional hydrogenation step[13] is expected to improve the mobility of polySi layers, boosting the *FF* and further enhancing the V_{OC}. The *EQE* of the best textured FSF-cell with NAOS/SiN_x passivation to the FSF is plotted in Fig. 5. The difference between the total absorptance $(1-R-T)$ and the *EQE* comes from carrier recombination and the parasitic absorption in (i) the front SiN_x, (ii) the doped polySi layers, and (iii) the metal contacts.

By looking at results reported in Table I, the FSF is the layer that exhibits the highest recombination rate, limiting the final V_{OC} and J_{SC}. Using only NAOS/SiN_x as front-side passivation stack, a fabricated cell with No-FSF/NAOS/SiN_x exhibited V_{OC} of 686 mV. To further improve the front-side passivation, the NAOS/SiN_x stack was then replaced by high-quality dry thermal-SiO_2/SiN_x stack. For this additional solar cell with No-FSF/dry-SiO_2/SiN_x, a V_{OC} of 696 mV was reached. In these two No-FSF cells, no improvement on the final conversion efficiency was observed mainly due to somewhat low *FF* (~72%) and J_{SC} (~37 mA/cm^2). These two aspects call for the abovementioned hydrogenation step aimed at polySi mobility enhancement (higher *FF*) as well as for a different rear design aimed to improve carriers collection (higher J_{sc}). Nevertheless, V_{OC}'s close to QSSP-based iV_{oc}'s were measured, indicating that our IBC architecture has the potential to reach efficiencies well beyond 22%.

We have presented ion-implanted polySi tunneling oxide passivating contacts applied into IBC solar cells. This represents a promising way for the design and realization of highly efficient solar cell. Both n-type and p-type passivating contacts in the cells have been prepared with local ion-implantation of LPCVD intrinsic polySi layers. The impact of doping profile of the passivating contacts on their passivation quality has been studied. It is found that, by precisely confining the implanted dopants within the polySi layers, an excellent surface passivation with iV_{oc} of 721 mV for n-type and 692 mV for p-type passivating contacts can be achieved (see Table I). The doping profile can be controlled by modifying the polySi layer thickness, the energy and dose of the ion-implantation, and the temperature and time of the annealing. Our best IBC solar cell with polySi passivating contacts presents an efficiency of 19.2%, with $V_{oc} = 673$ mV, $FF = 75.2\%$, and $pFF = 83.2\%$. By improving the front-side passivation, a V_{OC} of 696 mV was achieved. Further optimization of the polySi layers, rear design, the p/n gap, metal coverage at the rear side of the cell, and the passivation of the front-side will improve the solar cell performance.

This work was carried out with a subsidy of the Dutch Ministry of Economic Affairs (TKI Solar Energy—IBChampion project). The authors thank Ard Vlooswijk from the Tempress Systems BV for the ECV measurements and discussions.

[1]A. Cuevas, paper presented at the 42nd IEEE Photovoltaic Specialists Conference, New Orleans, LA, June 2015.
[2]M. Taguchi, A. Yana, S. Tohoda, K. Matsuyama, Y. Nakamura, T. Nishiwaki, K. Fujita, and E. Maruyama, J. Photovoltaics **4**, 96 (2014).
[3]E. Yablonovitch, T. Gmitter, R. M. Swanson, and Y. H. Kwark, Appl. Phys. Lett. **47**, 1211 (1985).
[4]F. Feldmann, M. Simon, M. Bivour, C. Reichel, M. Hermle, and S. W. Glunz, Appl. Phys. Lett. **104**, 181105 (2014).
[5]S. W. Glunz, F. Feldmann, A. Richter, M. Bivour, C. Reichel, H. Steinkemper, J. Benick, and M. Hermle, paper presented at the 31st European Photovoltaic Solar Energy Conference and Exhibition, Hamburg, September 2015.
[6]C. Reichel, F. Feldmann, R. Müller, A. Moldovan, M. Hermle, and S. W. Glunz, in *Proceedings of the 29th European PV Solar Energy Conference and Exhibition, Amsterdam, The Netherlands* (2014).
[7]U. Römer, R. Peibst, T. Ohrdes, B. Lim, J. Krügener, T. Wietler, and R. Brendel, IEEE J. Photovoltaics **5**(2), 507 (2015).
[8]D. L. Young, W. Nemeth, V. LaSalvia, R. Reedy, S. Essig, N. Bateman, and P. Stradins, IEEE J. Photovoltaics **6**, 41 (2015).
[9]C. Reichel, F. Feldmann, R. Müller, R. C. Reedy, B. G. Lee, D. L. Young, P. Stradins, M. Hermle, and S. W. Glunz, J. Appl. Phys. **118**, 205701 (2015).
[10]A. Ingenito, O. Isabella, and M. Zeman, international patent application, 016047 WO (2015).
[11]R. A. Sinton and A. Cuevas, Appl. Phys. Lett. **69**, 2510 (1996).
[12]F. Feldmann, R. Muller, C. Reichel, and M. Hermle, Phys. Status Solidi RRL **8**, 767 (2014).
[13]S. Lindekugel, H. Lautenschlager, T. Ruof, and S. Reber, in *Proceedings of the 23rd European PV Solar Energy Conference and Exhibition, Valencia, Spain* (2008).